Ultraconfined oblate hard particles between hybrid penetrable walls.

ANQUETIL-DECK, C., CLEAVER, Doug <http://orcid.org/0000-0002-4278-0098> and TEIXEIRA, P.I.C

Physical Review E **110**, 034705 (2024) DOI: 10.1103/PhysRevE.110.034705

Ultraconfined oblate hard particles between hybrid penetrable walls

C. Anquetil-Deck*

Department of Energy and Process Engineering, Norwegian University of Science and Technology, Høgskoleringen 5, NO–7491 Trondheim, Norway

D. J. Cleaver†

Materials and Engineering Research Institute, Sheffield Hallam University Pond Street, Sheffield S1 1WB, United Kingdom

P. I. C. Teixeira‡

ISEL – Instituto Superior de Engenharia de Lisboa, Instituto Politécnico de Lisboa Rua Conselheiro Emídio Navarro 1, 1959-007 Lisboa, Portugal and Centro de Física Teórica e Computacional, Faculdade de Ciências, Universidade de Lisboa, 1749-016 Lisboa, Portugal

(Dated: 26 September 2024)

Abstract

We have investigated, by Monte Carlo simulation, the orientational structure of very thin films of a discotic liquid crystal (DLC) confined between hybrid walls of controllable penetrability, as a function of wall separation L_z. Our purpose was to clarify whether, as predicted by continuum theory, the preferred orientation of the DLC is uniform, changes linearly, or changes discontinuously, when L_z and the anchoring strengths at either wall are changed. The model consists of oblate hard Gaussian overlap (HGO) particles: each wall sees a particle as a disc of zero thickness and diameter D less than or equal to that of the actual particle, σ_0, embedded inside the particle and located halfway along, and perpendicular to, its minor axis. This provides a particle-level mechanism to control the anchoring properties of the walls, from planar (edge-on) for $D \sim 0$ to homeotropic (face-on) for $D \sim \sigma_0$, which can be done independently at either wall. As in our earlier work [C. Anquetil-Deck *et al.*, J. Phys. Chem. B **124**, 7709–7716 (2020)], which was restricted to $L_z = 6\sigma_0$, depending on the values of $D_s \equiv D/\sigma_0$ at the top (D_s^t) and bottom (D_s^b) walls, we find domains in (D_s^b, D_s^t) space in which particle alignment is uniform planar (UP), uniform homeotropic (UH), or varies linearly from planar at one wall to homeotropic at the other (L), but no bistable or tristable regions are identified between these domains. Most importantly, there appears never to occur an abrupt change of the LC orientation when the walls strongly favour different anchorings, in general agreement with the scenario proposed by Velasco and co-workers [D. de las Heras *et al.*, Phys. Rev. E **79**, 011712 (2009)], but in contrast to the behaviour of equivalent calamitic systems [F. Barmes and D. J. Cleaver, Phys. Rev. E **69**, 061705 (2004); *ibid.* **71**, 021705 (2005); C. Anquetil-Deck *et al.*, Phys. Rev. E **86**, 041707 (2012)]. However, for the thinnest films investigated ($L_z = 2\sigma_0$), the system is unable to accommodate a rotation of the preferred particle orientation from one wall to the other and adopts instead a tilted configuration, similar to that reported earlier for Gay-Berne films in symmetric confinement [T. Gruhn and M. Schoen, Thin Solid Films **330**, 46–58 (1998); Mol. Phys. **93**, 681–692 (1998)] but which, as far as we know, has been missed in most earlier work.

*Electronic address: candy.deck@ntnu.no

†Electronic address: D.J.Cleaver@shu.ac.uk

‡Corresponding author. Telephone: +351 91 2668616; Electronic address: piteixeira@fc.ul.pt

I. INTRODUCTION

Recently there has been a surge of interest in the hitherto deemed exotic discotic liquid crystals (DLCs). These have now been realised experimentally for a huge variety of molecular shapes, including plates and discs [1], as well as at the colloidal level, e.g., in dispersions of gibbsite [2] or clay [3] particles. DLCs have potential applications in the photovoltaic industry, as they may exhibit semiconducting properties [4]. They are also effective as lubricants, outperforming hydrocarbons in some conditions [5]. On a more fundamental level, which interests us here, it is tempting to ask: in what ways do confined DLCs differ from their more conventional calamitic (i.e., composed of rod-shaped building blocks) counterparts? For it is well known that all current LC devices rely, for their operation, on the competing actions of bounding surfaces, known as anchoring, and of applied fields, on the preferred orientation of the LC particles, which makes it not improbable that the same will be true of future designs that use DLCs.

Typically the LC structure is strongly non-uniform close to surfaces, on lengthscales of the order of particle dimensions. At the most basic level, confinement can suppress the isotropic-nematic (I–N) transition altogether [6]. Far richer behaviour, however, is predicted to occur in hybrid films, where there are conflicting anchorings at either wall. Some 40 years ago, Barbero and Barberi [7] showed that a hybrid film with different surface anchoring strengths will adopt a bent-director, i.e., linear, configuration (L), where the nematic director rotates continuously between the walls, only if the film thickness is above some critical value set by the wall anchoring strengths and the Frank elastic constants of the nematic. In thinner films the director field is uniform (U), with the nematic director along the easy axis of the wall with stronger anchoring. Later, Palffy-Muhoray *et al.* [8] predicted that a very thin hybrid film with equally strong surface anchorings will adopt a step-like configuration (S), in which the director is uniform and along the wall-imposed direction in either half of the film, with a discontinuity around the film midplane, as the energy cost of this wall defect is less than the elastic energy cost of deforming the director continuously. This structure has been called eigenvalue-exchange or order reconstruction. The effects of different anchoring strengths at either wall, as well as of biaxiality, were investigated by Galabova *et al.* [9], who found a complex picture involving re-entrant transitions between the U, L and S configurations. These authors also noted that, if the anchoring strengths are different,

then the exchange region is located closer to the more weakly-anchoring wall. The problem was re-addressed later by Šarlah and Žumer [10], who also concluded that hybrid-anchored films with a thickness of only a few molecular lengths do not exhibit the continuous L structure. Qualitatively the same behaviour was found for a hybrid *twist* cell by Bisi *al.* [11], who carried out a detailed analysis of the relative stability of the different director configurations. All these studies have been performed using Landau-de Gennes theory, which makes no assumptions on the sizes or shapes of the LC building blocks; their findings are summarised in figure 1.

Monte Carlo (MC) simulations of a thin hybrid Lebwohl-Lasher film first appeared to confirm the above scenario [12], but later suggested a more complex picture whereby two transitions occur on lowering the temperature: first from the I phase to the S structure, and then to the L structure [13], However, Velasco *et al.* [14] using density-functional theory of a fluid of hard rods, proposed that, in the I phase of a hybrid cell, each wall is wetted by a uniform nematic layer of the appropriate orientation. As the I–N transition is approached, the layers grow from the walls into the bulk until they merge to give a linearly-rotating, bent-director profile. The I–N transition in a hybrid-aligned film is thus interpreted as the transition between a step-like, eigenvalue-exchange profile in the I phase and a linearly-rotating, bent-director profile in the N phase. A similar suggestion had actually been put forward earlier by Šarlah and Žumer [10], who argued that, because of the continuous growth of the ordered layers, there should be no I–N phase transition in a thin hybrid cell. Velasco *et al.* later performed very extensive and detailed MC simulations and mean-field calculations of the same system [15], which support Šarlah and Žumer's interpretation. In particular, they highlight the importance that the N phase should wet both walls: in the absence of complete N wetting at one wall, the S configuration morphs into something more akin to a U configuration dominated by the more strongly- anchoring wall, as first predicted by [7]. This leaves open the issue of the exact nature of the L–S transition that may have been observed experimentally [16].

As far as we are aware, these predictions have not been systematically checked against off-lattice computer simulations. This is one of our purposes. In an earlier paper [17], we reported a regime diagram for a fluid of confined oblate hard particles, comprising L, S and U phases, for a single film thickness. Here we complete our investigation by looking at film thicknesses ranging from quasi-two-dimensional (just two times the particle's diameter)

to quasi-bulk (nine times the particles's diameter). We place our results in the context of earlier work and discuss the meaningfulness of framing discussions of hybrid-confined LCs in terms of U, L and S configuratioons.

This paper is organised as follows: in section II we describe our model. We then give details of the computer simulations in section III, and present our results in section IV. We conclude in section V.

II. MODEL

As in previous work [17–21], we consider a purely steric microscopic model of uniaxial particles represented by the hard Gaussian overlap (HGO) potential [22]:

$$U^{HGO} = \begin{cases} 0 & \text{if } r_{ij} \geq \sigma(\hat{\mathbf{r}}_{ij}, \hat{\mathbf{u}}_i, \hat{\mathbf{u}}_j) \\ \infty & \text{if } r_{ij} < \sigma(\hat{\mathbf{r}}_{ij}, \hat{\mathbf{u}}_i, \hat{\mathbf{u}}_j) \end{cases},$$

where $\hat{\mathbf{u}}_i$ and $\hat{\mathbf{u}}_j$ are the orientations of particles i and j, $\hat{\mathbf{r}}_{ij}$ is the inter-particle unit vector, and $\sigma(\hat{\mathbf{r}}_{ij}, \hat{\mathbf{u}}_i, \hat{\mathbf{u}}_j)$ is the contact distance, given by

$$\sigma(\hat{\mathbf{r}}_{ij}, \hat{\mathbf{u}}_i, \hat{\mathbf{u}}_j) = \sigma_0 \left[1 - \frac{\chi}{2} \left[\frac{\left(\hat{\mathbf{r}}_{ij}.\hat{\mathbf{u}}_i + \hat{\mathbf{r}}_{ij}.\hat{\mathbf{u}}_j\right)^2}{1 + \chi(\hat{\mathbf{u}}_i.\hat{\mathbf{u}}_j)} + \frac{\left(\hat{\mathbf{r}}_{ij}.\hat{\mathbf{u}}_i - \hat{\mathbf{r}}_{ij}.\hat{\mathbf{u}}_j\right)^2}{1 - \chi(\hat{\mathbf{u}}_i.\hat{\mathbf{u}}_j)} \right] \right]^{-1/2}. \tag{1}$$

The parameter χ is set by the particle length-to-breadth ratio $\kappa = \sigma_L/\sigma_0$ via

$$\chi = \frac{\kappa^2 - 1}{\kappa^2 + 1}. \tag{2}$$

In this study, we consider disc-shaped, i.e., $\kappa < 1$ particles. For moderate κ, the HGO model is a good approximation to hard ellipsoids (HEs) [23–25]; furthermore, their virial coefficients (and thus their equations of state, at least at low to moderate densities) are very similar [26, 27]. From a computational point of view, HGOs have the considerable advantage over HEs that the distance of closest approach between two particles is given in closed form [28]. Particle–wall interactions are now modelled, as in [29], by a hard disc–wall (HDW) potential (see figure 2):

$$\beta\mathcal{V}^{HDW}(z, \theta) = \begin{cases} 0 & \text{if } |z - z_0^\alpha| \geq \frac{1}{2} D \sin\theta \\ \infty & \text{if } |z - z_0^\alpha| < \frac{1}{2} D \sin\theta \end{cases} \tag{3}$$

where $\beta = 1/k_{\mathrm{B}}T$, θ is the polar angle of the HGO orientation vector, and the z-axis has been chosen to be perpendicular to the walls, located at $z = z_0^{\alpha}$ ($\alpha = 1, 2$). According to equation (3), particles see each other as HGOs, but the walls see a particle as an infinitely thin disc of diameter D (which need not be the same at both walls, or in different regions of each wall). This is the oblate-particle version of the hard needle-wall potential of our earlier work [18–20, 30]: physically, $0 < D < \sigma_0$ means that the particles are able to embed their side- and end groups, but not the whole width of their cores, into the bounding walls. In an experimental situation, this might be achieved by manipulating the density, orientation or chemical affinity of an adsorbed surface layer: in other words, we are able to model different *surfaces* by changing a property of the *particles* that only the surfaces 'see'. Other, formally simpler, but in our view no more realistic, choices would be a Rapini-Papoular-like interaction as in, e.g., [14], or just plain excluded volume [31]. In what follows, the particle-wall interaction is characterised using the dimensionless parameter $D_s = D/\sigma_0$; as shown in [17, 21], this allows us to set the anchoring at either wall as either homeotropic (face-on) for $D_s \lesssim 1$, or planar degenerate (edge-on) for $D_s \ll 1$), although anchoring *strengths* cannot be finely controlled thus.

III. SIMULATIONS

The effect of confinement was studied by performing NVT MC simulations of HGO particles of length-to-breadth ratio $\kappa = 0.345$, sandwiched between two hybrid walls a distance L_z apart. Periodic boundary conditions were imposed in the x and y directions. The reduced bulk density $\rho^* = \rho\sigma_0^3$ (which we shall often refer to as 'bulk density' or simply 'density') is defined as just the number of particles divided by the volume of the simulation box: it is not the density of the bulk fluid coexisting with the confined fluid. Each system was initialised at a low density ($\rho^* = 1.5$) and gently compressed by decreasing the box dimensions L_x and L_y while keeping the wall separation L_z fixed. At each density, each particle was selected sequentially and an attempt was made to displace and rotate it at random; this is an MC sweep, which is accepted or rejected using a no-overlap criterion. Maximum translational and rotational displacement parameters were allowed to vary during the equilibration stage to yield acceptance ratios of approximately 50%. Run lengths of one million MC sweeps were performed, averages and profiles being accumulated for the final

500 000 sweeps. It is difficult to say how long a run needs to be to guarantee equilibration, but blocks of $500 - 1000$ time steps or MC cycles are typical (for an N-particle system, one MC cycle consists of N sweeps) [32]. For our system, 500 000 sweeps were performed during equilibration, which is in line with the above: a system composed of 864 HGO particles is estimated to need between 432 000 and 864 000 sweeps to reach equilibration. Analysis has been performed by dividing the stored system configurations into n_z equidistant constant-z slices and calculating averages of relevant observables in each slice. This yields profiles of quantities such as the number density $\rho^*(z)$, from which structural changes can be assessed. The orientational order parameter tensor $Q(z)$ has also been calculated, in particular

$$\langle Q_{zz}(z) \rangle = \frac{1}{N(z)} \sum_{i=1}^{N(z)} \left(\frac{3}{2} \cos^2 \theta_i(z) - \frac{1}{2} \right), \tag{4}$$

which measures the variation across the confined films of orientational order measured with respect to the wall normal. This is significantly less sensitive to finite-size effects than $P_2(z)$, the order parameter in the director frame. Here $N(z)$ is the instantaneous occupancy of the relevant slice and θ_i is the angle between the wall normal (i.e., the z-axis) and the particle orientation $\hat{\mathbf{u}}_i$. Q_{zz}, as usual, tells us whether alignment is homeotropic ($Q_{zz} > 0$) or planar ($Q_{zz} < 0$). To quantify any possible biaxiality, we start by noting that, typically, one of the eigenvalues of the full order parameter tensor $Q(z)$ is much larger (in absolute value) than the other two. This we call the leading eigenvalue. The two non-leading eigenvalues are either identical, if there is no biaxiality, or they differ by an amount that is less (again, in absolute value) than the difference between either of them and the leading eigenvalue. Thus we have elected to define a biaxial order parameter $\Delta(z)$ as the absolute value of the difference of the two non-leading eigenvalues of $Q(z)$.

Table I collects the numbers of particles and of slices for the six systems studied. We have checked for finite-size effects by re-running our simulations with double the number of particles for a few $L_z = 2\sigma_0$ systems, and found no significant differences.

IV. RESULTS

All results presented are for $\kappa = 0.345$ and substrate separation $2\sigma_0 \leq L_z \leq 9\sigma_0$. We also did a few runs for $L_z = 12\sigma_0$, which revealed no qualitative, and few quantitative, differences to those for $L_z = 9\sigma_0$. In what follows, D_s^b and D_s^t denote, respectively, the dimensionless

thin disc diameter at the bottom (left in figures) and top (right in figures) substrate.

Figure 3 shows the reduced density $\rho^*(z)$ the order parameter with respect to the substrate normal $Q_{zz}(z)$, and the biaxial order parameter $\Delta(z)$, for the most extreme case of asymmetric confinement, corresponding to $D_s^b = 1.0$ and $D_s^t = 0.0$ and wall separations $L_z/\sigma_0 = 9$, 6, 3 and 2. For all L_z, at the lowest bulk density $\rho\sigma_0^3 = 1.6$, corresponding to the I phase, there is strong face-on alignment at the left wall, and moderate edge-on alignment at the right wall, separated by a disordered bulk. Then as the density is increased through the I–N transition ($\rho\sigma_0^3 = 2.5$) and into the N phase ($\rho\sigma_0^3 = 3.1$), edge-on alignment is enhanced at the right wall, and simultaneously $Q_{zz}(z)$ acquires a roughly linear shape as a function of z, albeit with oscillations that are more pronounced for the two thinner systems ($L_z/\sigma_0 = 3$ and 2). So it is noteworthy that something one might reasonably call an L configuration survives all the way down to $L_z/\sigma_0 = 2$, i.e., very strong confinement, although in this limit there is non-negligible biaxiality at the right (planar-aligning) wall. The overall picture is consistent with Velasco *al.*'s scenario [14, 15] that the S–L transition coincides with the bulk I–N transition. In particular, there does not appear to be any S configuration where the homeotropically- and planar-aligned layers touch. Similar results are obtained for less extreme instances of asymmetric confinement.

Figures 4 ($D_s^b = 1.0$, $D_s^t = 0.7$) and 5 ($D_s^b = 0.2$, $D_s^t = 0.0$) show $\rho^*(z)$, $Q_{zz}(z)$ and $\Delta(z)$ for UH and UP configurations, respectively, for the same set of wall separations as in figure 3. Figure 4 exhibits a very strong and fairly uniform face-on (homeotropis) alignment at the highest bulk density, but only a moderate amount of layering, which extends about $1.5\sigma_0$ from either wall, and essentially no biaxiality. In contrast, in figure 5 alignment is edge-on (planar) almost everywhere, except for a very small number of particles located very close to the left, or bottom, wall, where it is face-on (homeotropic). For all wall separations there is well-defined layering, as evidenced by the very sharp density peaks. The number of 'bulk' density peaks (i.e., excluding those located right next to the walls) equals L_z/σ_0 if this is 9, 6 or 5, and $L_z/\sigma_0 - 1$ otherwise (results for $L_z/\sigma_0 = 4$ and 5 not shown), indicating layer stratification in the three thicker films (as also seen in thin films of Gay-Berne particles adsorbed at a flat wall in the presence of a coexisting vapour phase [33]) but not so much so in the three thinner ones. The two thinner films ($L_z/\sigma_0 = 2$ and 3) also exhibit a fair amount of biaxiality in the N phase, which is absent in the thicker films. Finally, the Q_{zz} profiles for the thinnest films studied ($L_z/\sigma_0 = 2$) are noticeably less smooth than for their

thicker counterparts, which we attribute to the very long-lived orientational domains that can develop in these highly confined systems.

Figure 6 summarises our findings in (D_s^b, D_s^t) space. It is seen that, for all L_z, UP (edge-on) alignment dominates when D_s^b and D_s^t are both substantially smaller than 1, whereas UH (face-on) alignment is obtained for D_s^b and D_s^t both close to 1. When $D_s^b \gg D_s^t$ ($D_s^b \ll D_s^t$), there is homeotropic alignment at the bottom (top) substrate and planar alignment at the top (bottom) substrate, and the direction of preferential alignment rotates linearly from one substrate to the next (L). Remarkably, there appears to be no substantial shrinking of the L region with decreasing L_z. Contrary to our earlier conjecture, no bistable or tristable states were found akin to those reported by some of us for prolate HGOs confined between either uniform [31, 34] or square-patterned [35] substrates using the hard needle-wall potential. In general terms we confirm the scenario of Velasco *et al.* [14, 15] that, for walls that favour antagonistic anchorings sufficiently strongly, the S–L transition coincides with the I–N transition and there is no S configuration. Interestingly, however, the thinnest films investigated ($L_z/\sigma_0 = 2$) are unable to accommodate a rotation of the preferred particle orientation from one wall to the other and adopt instead a tilted (T) configuration (see figure 7). Perhaps unexpectedly, this seems to be only weakly biaxial, even at the highest densities investigated. A similar finding was reported earlier by Gruhn and Schoen for Gay-Berne films in symmetric confinement [36, 37], but does not seem to have received much attention.

V. CONCLUSIONS

We have simulated a fluid of oblate HGO particles confined in a slit geometry with hybrid anchoring boundary conditions. The anchoring can be tuned at either substrate, by varying the extent to which a particle is allowed to penetrate it. This extends our earlier work [17] by considering a number of (small) slit widths/film thicknesses L_z. As before, [17], we found that, if the anchorings at the two substrates are not too different, then a state of uniform alignment, either planar (UP) or homeotropic (UH) is realised. Otherwise there is a linear variation from planar alignment at one substrate to homeotropic alignment at the other. The exception to the latter is the very thinnest films $L_z/\sigma_0 = 2$), for which the LC adopts a uniform tilted configuration which does not satisfy the anchorings at either wall, as to do

so would lead to extremely strong distortions. Moreover, we are now able to rule out, with reasonable confidence, the existence of regions of bistability, or even of tristability between the UH, UP and L domains, where the configuration that is actually realised might depend on system history and/or initial conditions.

The rich behaviour described above lies beyond the capabilities of both Landau-de Gennes theory, which has been most often used to study hybrid films, and, as noted in [17], of Onsager's second-virial approximation of density-functional theory (DFT). A more sophisticated approach is required, perhaps along the lines of Schmidt's fundamental-measure DFT [38]. This might be combined with a machine-learning method, e.g., a neural network, for searching for the free energy minimum, as earlier proposed by us [39].

Data availability statement

The data that support the findings of this study are available from the corresponding author upon reasonable request.

Acknowledgements

We acknowledge financial support from the Fundação para a Ciência e a Tecnologia under grants no. UIDB/00618/2020 (DOI: 10.54499/UIDB/00618/2020) and no. UIDP/00618/2020 (DOI: 10.54499/UIDP/00618/2020).

[1] C. Tschierske, Micro-Segregation, Molecular Shape and Molecular Topology – Partners for the Design of Liquid Crystalline Materials with Complex Mesophase Morphologies, J. Mater. Chem. **11**, 2647–2671 (2001).

[2] F. M. van der Kooij and H. N. W. Lekkerkerker, Formation of Nematic Liquid Crystals in Suspensions of Hard Colloidal Platelets, J. Phys. Chem. B **102**, 7829–7832 (1998).

[3] C. Pizzey, J. S. van Duijneveldt and S. Klein, Liquid Crystal Clay Composites, Mol. Cryst. Liq. Cryst. **409**, 51–57 (2004).

[4] C. Zou, J. Wang, M. Wang, Y. Wu, K. Gu, Z. Shen, G. Xiong, H. Yang, L. Jiang and T. Ikeda, Patterning of Discotic Liquid Crystals with Tunable Molecular Orientation for Electronic Applications, Small **14**, 1800557 (2018).

[5] R. J. Bushby and K. Kawata, Liquid Crystals that Affected the World: Discotic Liquid Crystals, Liq. Cryst. **38**, 1415–1426 (2011).

[6] P. Sheng, Boundary-layer phase transition in nematic liquid crystals, Phys. Rev. A **26**, 1610–1617 (1982).

[7] G. Barbero and R. Barberi, Critical thickness of a hybrid aligned nematic liquid crystal cell, J. Phys. (Paris) **44**, 609–616 (1983).

[8] P. Palffy-Muhoray, E. C. Gartland, and J. R. Kelly, A new configurational transition in inhomogeneous nematics, Liq. Cryst. **16**, 713–718 (1994).

[9] H. G. Galabova, N. Kothekar and D. W. Allender, Stable configurations in hybrid nematic cells in relation to thickness and surface order, Liq. Cryst. **23**, 803–811 (1997).

[10] A. Šarlah and S. Žumer, Equilibrium structures and pretransitional fluctuations in a very thin hybrid nematic film, Phys. Rev. E **60**, 1821–1830 (1999).

[11] F. Bisi, E. C. Gartland, R. Rosso and E. G. Virga, Order reconstruction in frustrated nematic twist cells, Phys. Rev. E **68**, 021707 (2003).

[12] C. Chiccoli, P. Pasini, A. Šarlah, C. Zannoni and S. Žumer, Structures and transitions in thin hybrid nematic films: A Monte Carlo study, Phys. Rev. E **67**, 050703(R) (2003).

[13] C. Chiccoli, S. P. Gouripeddi, P. Pasini, R. P. N. Murthy, V. S. S. Sastry and C. Zannoni, Hybrid Nematic Films: A Detailed Monte Carlo Investigation, Mol. Cryst. Liq. Cryst. **500**, 118–131 (2009).

[14] D. de las Heras, L. Mederos and E. Velasco, Capillary and anchoring effects in thin hybrid nematic films and connection with bulk behavior, Phys. Rev. E **79**, 011712 (2009).

[15] R. G. Marguta, Y. Matínez-Ratón, N. G. Almarza, and E. Velasco, Theory and simulation of the confined Lebwohl-Lasher model, Phys. Rev. E **83**, 041701 (2011).

[16] B. Zappone, Ph. Richetti, R. Barberi, R. Bartolino and H. T. Nguyen, Forces in nematic liquid crystals constrained to the nanometer scale under hybrid anchoring conditions, Phys. Rev. E **71**, 041703 (2005).

[17] C. Anquetil-Deck, D. J. Cleaver and P. I. C. Teixeira, Ordering of Oblate Hard Particles between Hybrid Penetrable Walls, J. Phys. Chem. B **124**, 7709–7716 (2020).

[18] P. I. C. Teixeira, F. Barmes and D. J. Cleaver, Symmetric alignment of the nematic matrix between close penetrable colloidal particles, J. Phys.: Condens. Matter **16**, S1969 (2004).

[19] P. I. C. Teixeira, F. Barmes, C. Anquetil-Deck and D. J. Cleaver, Simulation and theory of hybrid aligned liquid crystal films, Phys. Rev. E **79**, 011709 (2009).

[20] P. I. C. Teixeira, Nematic Liquid Crystal Order Reconstruction in Ultraconfinement, From Density-Functional Theory, Liq. Cryst. **43**, 1526–1535 (2016).

[21] P. I. C. Teixeira, C Anquetil-Deck and D. J. Cleaver, Ordering of Oblate Hard Particles Between Symmetric Penetrable Walls, Liq. Cryst. **48**, 75–87 (2021).

[22] M. Rigby, Hard Gaussian Overlap Fluids, Mol. Phys. **68**, 687–697 (1989).

[23] J. W. Perram and M. S. Wertheim, Statistical Mechanics of Hard Ellipsoids: 1. Overlap Algorithm and the Contact Function, J. Comput. Phys. **58**, 409–416 (1985).

[24] M. P. Allen, G. T. Evans, D. Frenkel and B. M. Mulder, Hard Convex Body Fluids, Adv. Chem. Phys. **86**, 1–166 (1993).

[25] J. W. Perram, J. Rasmussen, E. Praestgaard and J. L. Lebowitz, Ellipsoid contact potential: Theory and relation to overlap potentials, Phys. Rev. E **54**, 6565–6573 (1996).

[26] V. R. Bhethanabotla and W. Steele, A Comparison of Hard-Body Models for Axially-Symmetrical Molecules, Mol. Phys. **60**, 249–251 (1987).

[27] S. L. Huang and V. R. Bhethanabotla, Virial Coefficients for the Hard Gaussian Overlap Model, Int. J. Mod. Phys. C **10**, 361–374 (1999).

[28] E. Velasco and L. A. Mederos, A Theory for the Liquid-Crystalline Phase Behavior of the Gay-Berne Model, J. Chem. Phys. **109**, 2361–2370 (1998).

[29] H. Reich and M. Schmidt, Capillary Nematization of Hard Colloidal Platelets Confined Between two Parallel Hard Walls, J. Phys. Condens. Matter **19**, 326103 (2007).

[30] D. J. Cleaver and P. I. C. Teixeira, Discontinuous Structural Transition in a Thin Hybrid Liquid Crystal Film. Chem. Phys. Lett. **338**, 1–6 (2001).

[31] F. Barmes and D. J. Cleaver, Using particle shape to induce tilted and bistable liquid crystal anchoring, Phys. Rev. E **71**, 021705 (2005).

[32] M. P. Allen and D. J. Tildesley, *Computer Simulation of Liquids* (Oxford University Press, Princeton, 1987).

[33] G. D. Wall and D. J. Cleaver, Computer simulations of adsorbed liquid crystal films, Mol. Phys. **101**, 1105–1112 (2003).

[34] F. Barmes and D. J. Cleaver, Computer simulation of a liquid-crystal anchoring transition, Phys. Rev. E **69**, 061705 (2004).

[35] C. Anquetil-Deck, D. J. Cleaver, and T. J. Atherton, Competing alignments of nematic liquid crystals on square-patterned substrates, Phys. Rev. E **86**, 041707 (2012).

[36] T. Gruhn and M. Schoen, Grand canocical ensemble Monte Carlo simulations of confined nematic Gay-Berne films, Thin Solid Films **330**, 46–58 (1998).

[37] T. Gruhn and M. Schoen, A grand canonical ensemble Monte Carlo study of confined planar and homeotropically anchored Gay-Berne films. Mol. Phys. **93**, 681–692 (1998).

[38] A. Esztermann, H. Reich, and M. Schmidt, Density Functional Theory for Colloidal Mixtures of Hard Platelets, Rods, and Spheres, Phys. Rev. E **73**, 011409 (2006).

[39] T. Santos-Silva, P. I. C. Teixeira, C. Anquetil-Deck, and D. J. Cleaver, Neural-network approach to modeling liquid crystals in complex confinement, Phys. Rev. E **89**, 053316 (2014).

L_z/σ_0	N	n_s
9	1372	150
6	864	100
5	720	83
4	576	66
3	432	50
2	288	33

TABLE I: Numbers of particles (N) and slices (n_z) for the six systems studied.

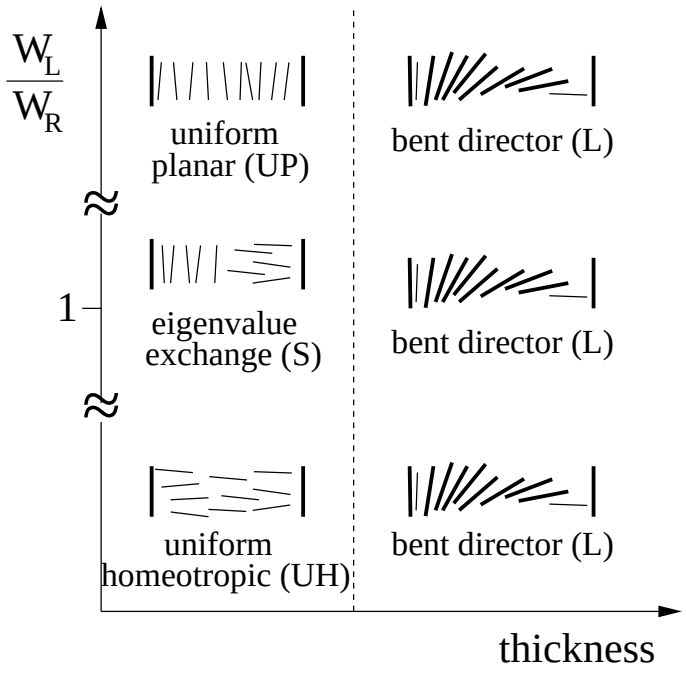

FIG. 1: Schematic diagram of the director configurations of a nematic LC film confined between a left wall that favours planar anchoring with strength W_L and a right wall that favours homeotropic anchorhing with strength W_R. The dashed line marks the critical thickness (in real systems this need not be vertical, or even straight).

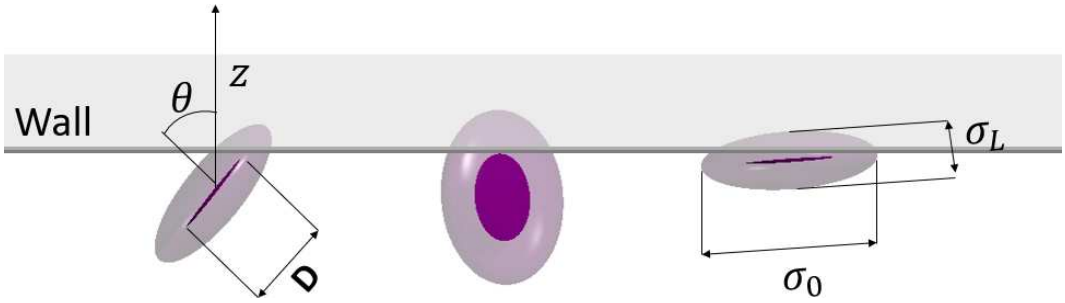

FIG. 2: The HDW potential: the wall sees a particle as a hard disc of diameter D, which need not equal σ_0 Varying D between 0 and σ_0 is equivalent to changing the degree of side-group penetrability into the confining walls, and hence the wall's anchoring properties.

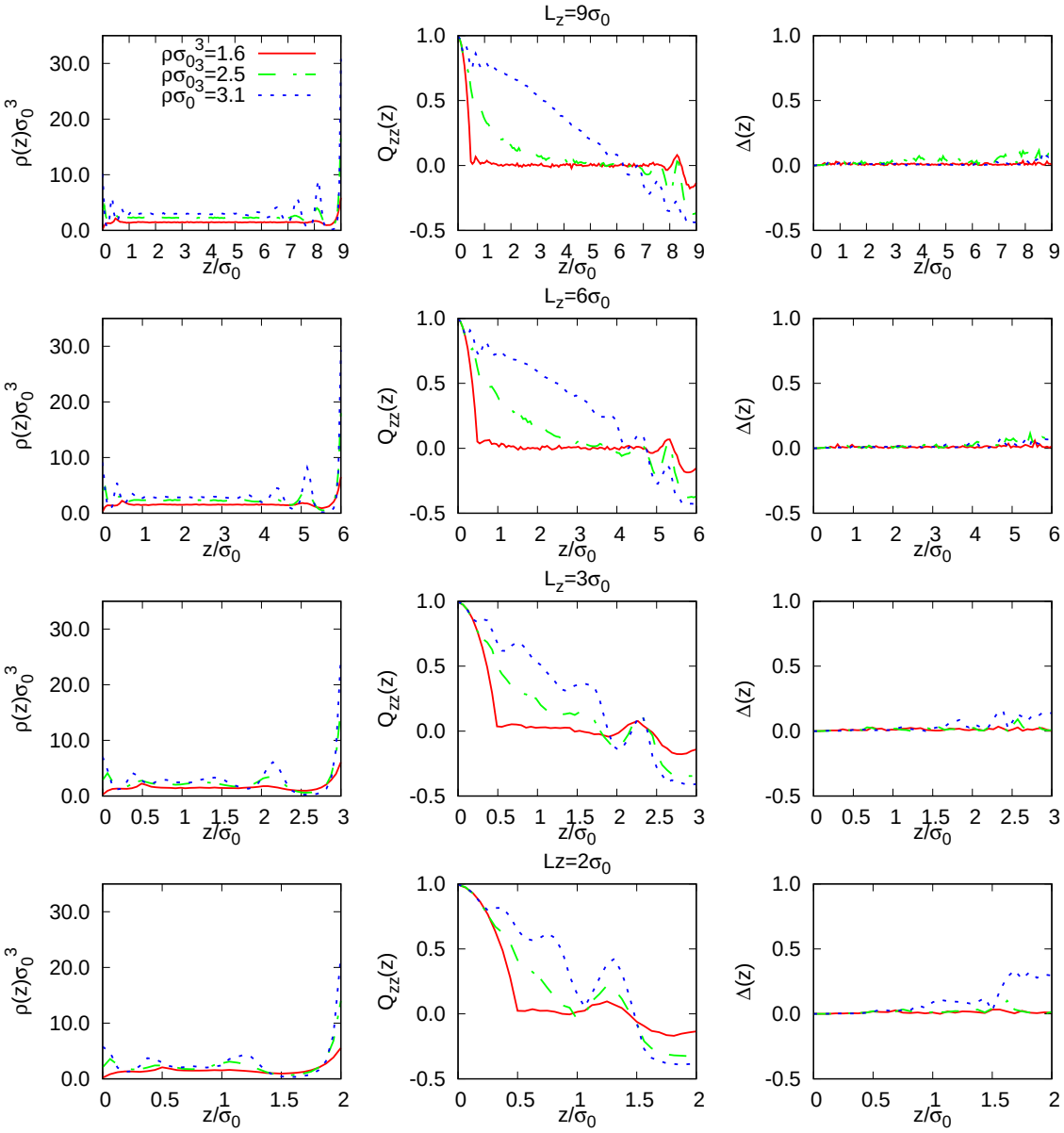

FIG. 3: Reduced density $\rho^*(z)$ (left column), order parameter with respect to the substrate normal $Q_{zz}(z)$ (middle column) and biaxial order parameter $\Delta(z)$ (right column) for $D_s^b = 1.0$ (left or bottom wall), $D_s^t = 0.0$ (right or top wall) and wall separations $L_z/\sigma_0 = 9$ (first row), 6 (second row), 3 (third row) and 2 (fourth row), at bulk densities $\rho\sigma_0^3 = 1.6$ (solid red curves), 2.5 (dot-dashed green curves) and 3.1 (short-dashed blue curves), corresponding to the I phase, I–N transition region, and N phase, respectively. This is the most extreme asymmetric confinement, yielding the L configuration.

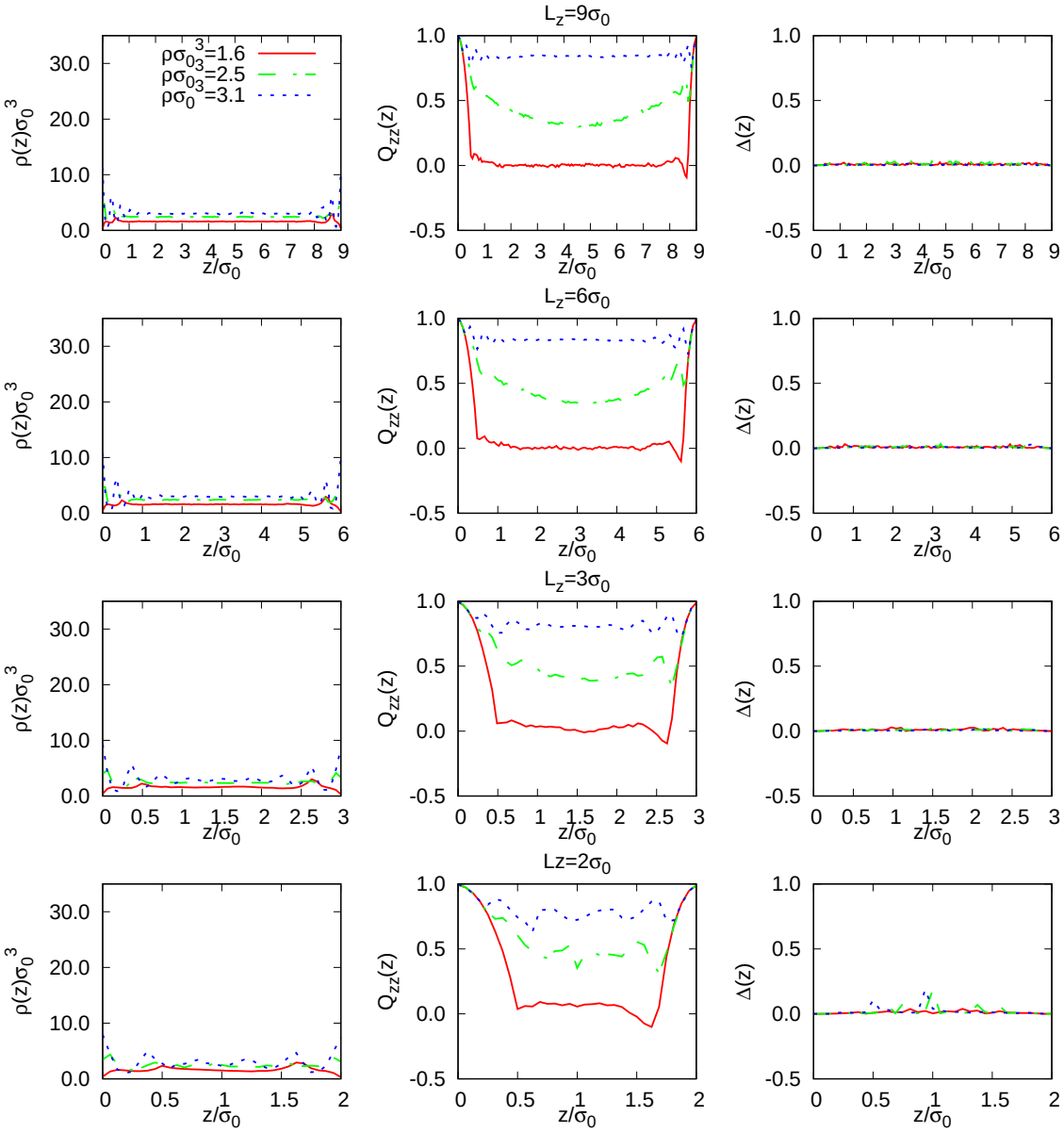

FIG. 4: Reduced density $\rho^*(z)$ (left column), order parameter with respect to the substrate normal $Q_{zz}(z)$ (middle column) and biaxial order parameter $\Delta(z)$ (right column) for $D_s^b = 1.0$ (left or bottom wall), $D_s^t = 0.7$ (right or top wall) and wall separations $L_z/\sigma_0 = 9$ (first row), 6 (second row), 3 (third row) and 2 (fourth row), at bulk densities $\rho\sigma_0^3 = 1.6$ (solid red curves), 2.5 (dot-dashed green curves) and 3.1 (short-dashed blue curves), corresponding to the I phase, I–N transition region, and N phase, respectively. This is the UH configuration.

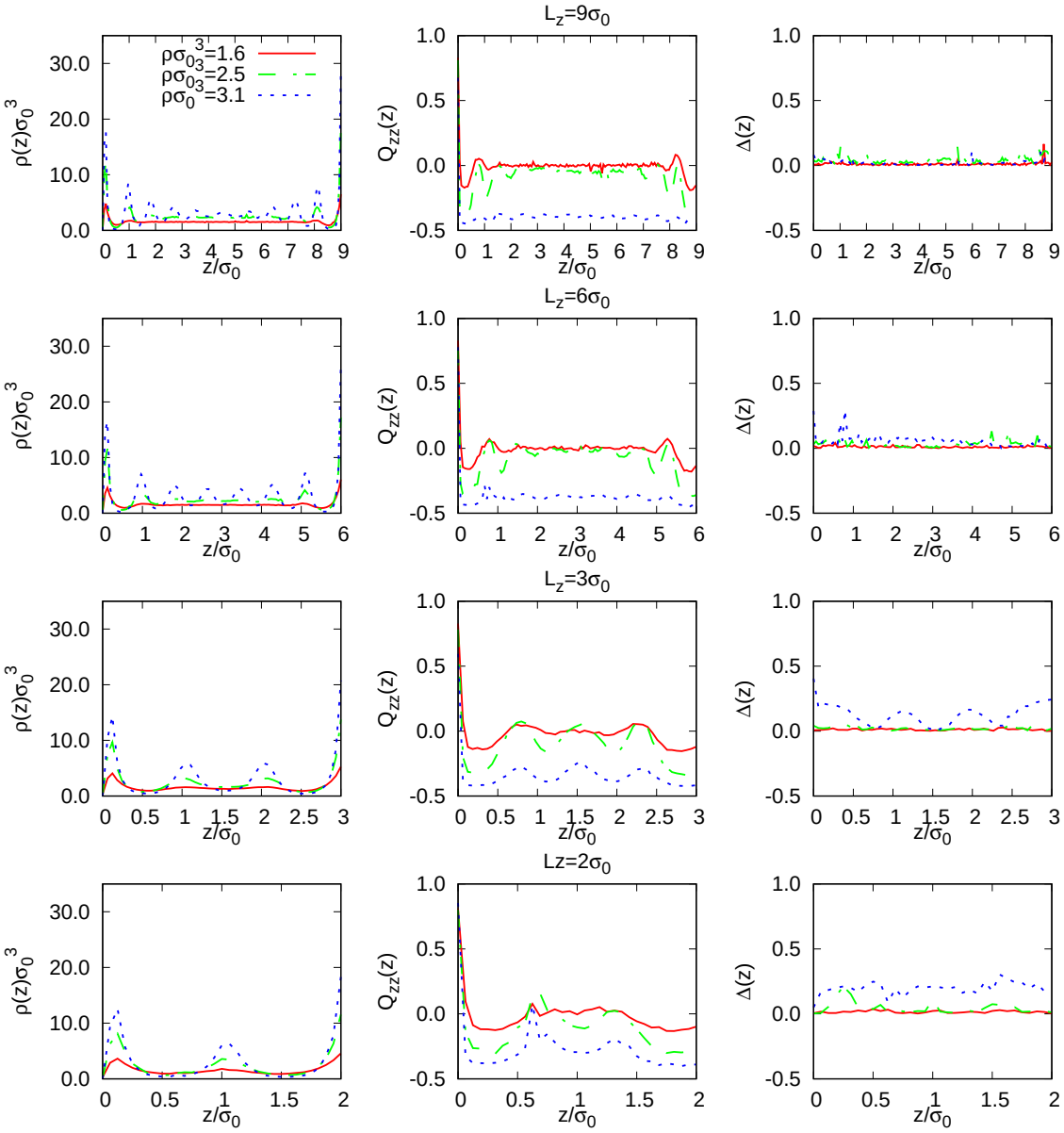

FIG. 5: Reduced density $\rho^*(z)$ (left column), order parameter with respect to the substrate normal $Q_{zz}(z)$ (middle column) and biaxial order parameter $\Delta(z)$ (right column) for $D_s^b = 0.2$ (left or bottom wall), $D_s^t = 0.0$ (right or top wall) and wall separations $L_z/\sigma_0 = 9$ (first row), 6 (second row), 3 (third row) and 2 (fourth row), at bulk densities $\rho\sigma_0^3 = 1.6$ (solid red curves), 2.5 (dot-dashed green curves) and 3.1 (short-dashed blue curves), corresponding to the I phase, I–N transition region, and N phase, respectively. This is the UP configuration.

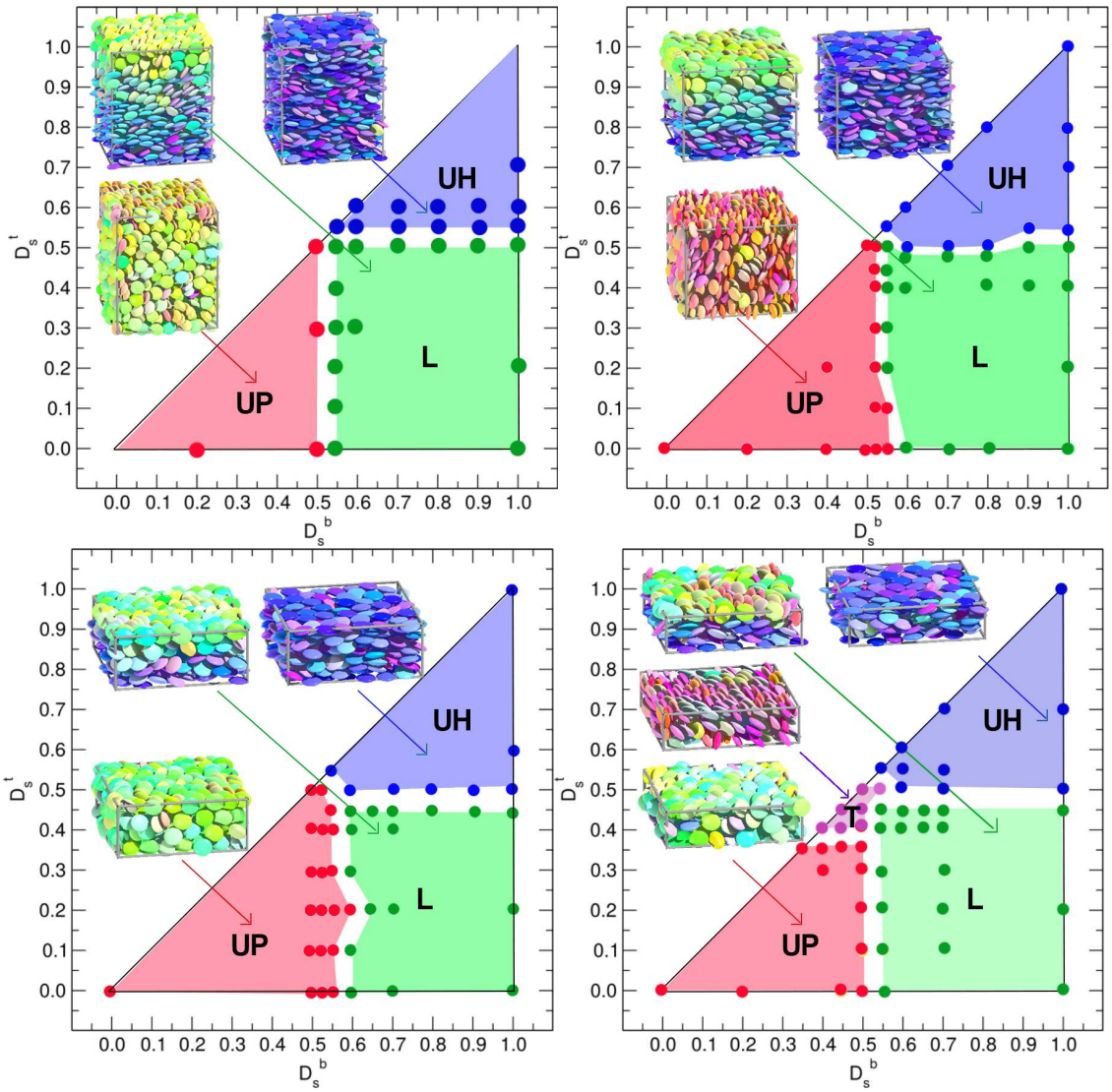

FIG. 6: Regime diagrams for a hybrid-confined HGO film of thicknesses $L_z = 9\sigma_0$ (top left), $L_z = 6\sigma_0$ (top right), $L_z = 3\sigma_0$ (bottom left) and $L_z = 2\sigma_0$ (bottom right). UH: uniform homeotropic (face-on); UP; uniform planar (edge-on); L: linear rotation from homeotropic to planar. The upper half of the diagrams can be obtained by exchanging D_s^b and D_s^t in the lower half, and is therefore not shown.

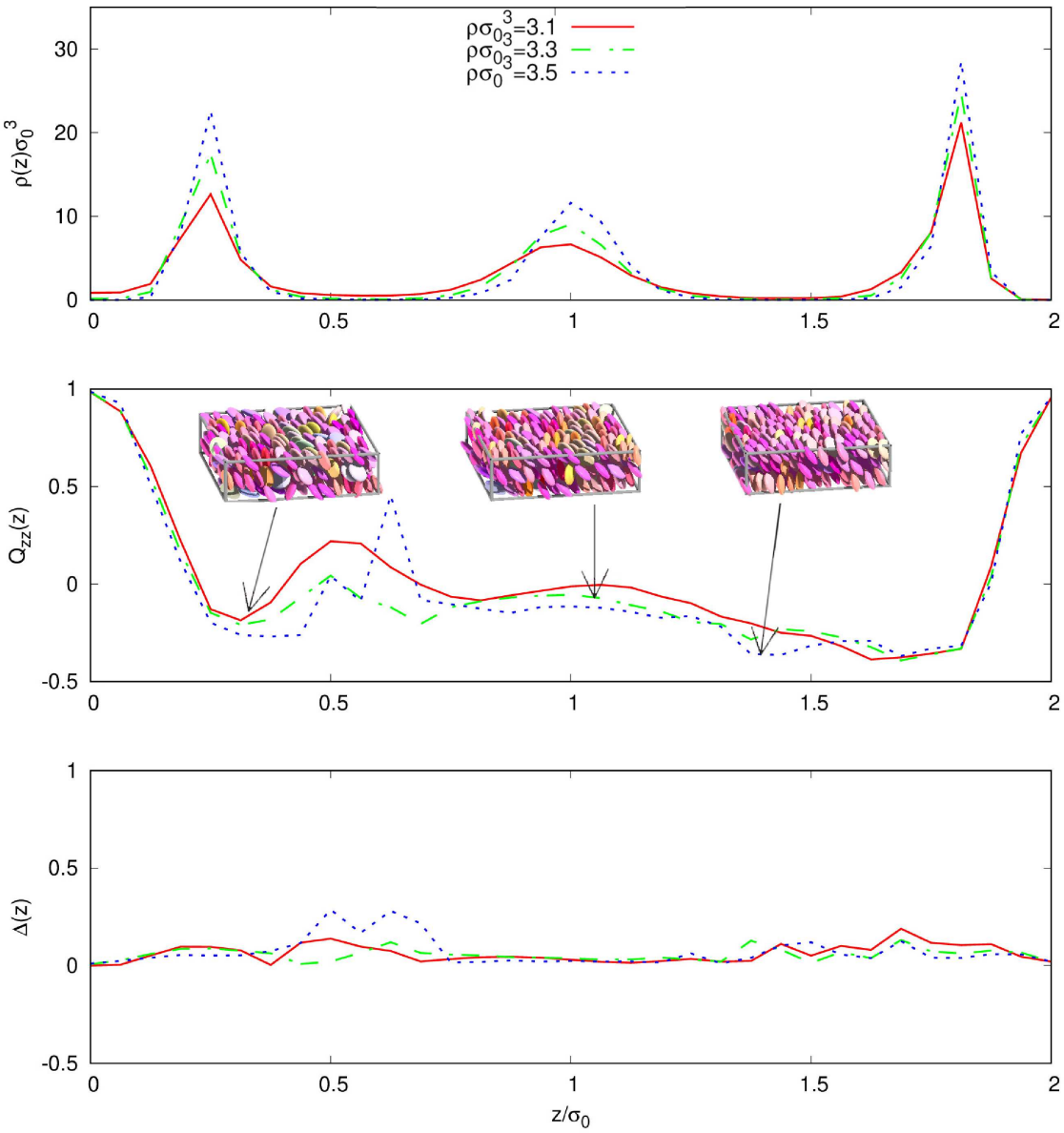

FIG. 7: Snapshots, $\rho^*(z)$ (top) $Q_{zz}(z)$ (middle) and $\Delta(z)$ (bottom) profiles of the thinnest system studied, $L_z = 2\sigma_0$, for $D_s^b = 0.55$ (left or bottom wall), $D_s^t = 0.4$ (right or top wall), showing the tilted (T) configuration obtained at bulk densities $\rho\sigma_0^3 = 3.1$, 3.3 and 3.5.